Chapter 3

Reconfigurable Intelligent Surface Assisted Downlink INOMA System*

*Part of this work has been published as:

M. Hemanta Kumar, Sanjeev Sharma, Kuntal Deka, and M. Thottappan. "Reconfigurable intelligent surface assisted downlink INOMA system", *Transactions on Emerging Telecommunications Technologies- Wiley.* 2022;e4537. doi: 10.1002/ett.4537.

3.1 Introduction

This chapter integrates RIS with NOMA to enhance spectral and energy efficiencies. Moreover, a downlink RIS-assisted index modulation NOMA for the next-generation wireless systems, referred to as R-INOMA has been proposed. In the present work, the cell-edge user (*user-1*) carries the information in the spatial domain using the transmitted antenna (TA) index, and the remaining NOMA users transmit information using constellation points with various power levels. Therefore, R-INOMA mitigates IUI among the users and serves more users in one resource block as compared to the conventional NOMA system. We summarize the main contributions of the chapter as follows:

- In this chapter, a RIS-assisted INOMA (R-INOMA) for a downlink system with one BS, and T number of cluster, each cluster consisting of three users are considered. The proposed novel R-INOMA system is more flexible, efficient, and supports more users with varying QoS (quality of service) than the individual NOMA or I-NOMA.
- The proposed R-INOMA system aims to decrease IUI among the users and enhances the spectral and energy efficiencies.
- The diversity order of the proposed is analyzed system and derived an upper bound on the probability of error.
- The analysis of the proposed system design in terms of symbol error rate, diversity order and the sum-rate over Rayleigh fading channels is carried out, and also compared with conventional NOMA and IM-NOMA-based systems. The simulation results show that the proposed R-INOMA system achieves a

better BER at low SNR due to the effect of passive reflecting elements, and it is also verified analytically.

- Further, the impact of transmitting and receiving antennas, reflecting elements, imperfect channel, and modulation order is studied in the proposed R-INOMA.
- BER is also computed in Rician fading channel scenario and compared with Rayleigh fading channel.
- Finally, the effect of imperfect SIC and energy efficiency analysis is considered in the proposed system.

This chapter is organized as follows. In Section 3.2, the proposed RIS-assisted downlink INOMA system is presented. The analytical expressions of BEP performance is presented in Section 3.3. Analytical and simulation results are presented in Section 3.4, and the summary of the proposed work is discussed in Sections 3.5.

3.2 Proposed R-INOMA System Model

In the present work, RIS-assisted downlink INOMA (R-INOMA) is considered, as shown in Figure 3.1, In R-INOMA, each cluster has three users, and the BS is equipped with N_{t} transmit antennas and each user having N_{r} received antennas. Moreover, the BS communicates to users through RIS, a consisting of N passive reflecting elements. In Figure 3.1, IM is integrated with power domain NOMA (PD-NOMA) at BS, where the user $\mathcal{U}_1$ is assigned in the spatial domain and the remaining two users $\mathcal{U}_2$ and $\mathcal{U}_3$ are using the NOMA technique. NOMA users transmit the information using constellation points such as binary phase shift keying (BPSK).

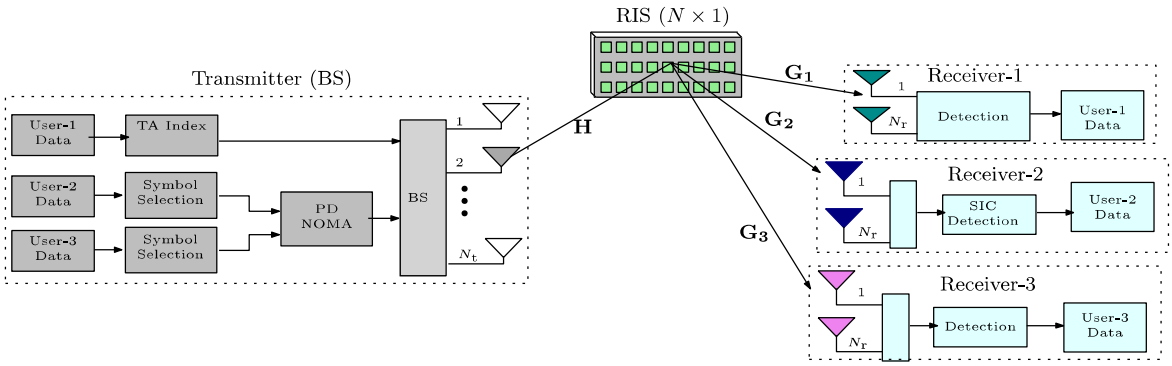

FIGURE 3.1: The proposed RIS-assisted INOMA (R-INOMA) system model.

Further, all the system parameters are defined in Table 3.1. The channel from the BS to RIS and RIS to users are denoted by $\mathbf{H} \in \mathbb{C}^{N \times N_t}$ and $\mathbf{G}_k \in \mathbb{C}^{N_r \times N}$, respectively, where $k = 1, 2, 3$. All the channels are flat Rayleigh fading which are independent and identically distributed (iid) with $\mathbf{H} \sim \mathcal{CN}(0, 1)$, and $\mathbf{G}_k \sim \mathcal{CN}(0, \sigma_k^2)$ [67]. The absolute channel gain of $\mathcal{U}_2$ is higher than the $\mathcal{U}_3$, i.e, $\|\mathbf{G}_2 \mathbf{\Phi} \mathbf{H}\| \gg \|\mathbf{G}_3 \mathbf{\Phi} \mathbf{H}\|$. Therefore, $\mathcal{U}_2$ and $\mathcal{U}_3$ are also referred to as near user (NU) and far user (FU), respectively.

The user-1 $\mathcal{U}_1$ transmits at the data rate $\log_2(N_t)$ bits per symbol and its transmit antenna (TA) index is expressed as,

$$\mathbf{x}_1 = [\underbrace{0, \ldots, 0}_{(t-1)}, 1, \underbrace{0, \ldots 0}_{(N_t - t)}]^T. \tag{3.1}$$

Therefore, $\mathbf{x}_1$ has only t^{th} index position '1' and the remaining elements are zeros. NOMA users $\mathcal{U}_2$ and $\mathcal{U}_3$ transmit at data rate $\log_2(\mathrm{M})$, where M denotes the modulation order, using activated TA by $\mathcal{U}_1$, and the superposed signal at BS is given by

$$\mathbf{x} = [\underbrace{0, \ldots, 0}_{(t-1)}, \mathcal{S}, \underbrace{0, \ldots 0}_{(N_t - t)}]^T, \in \mathbb{C}^{N_t \times 1} \tag{3.2}$$

where, $\mathcal{S} = \sqrt{a_1 \mathrm{P}_b} x_2 + \sqrt{a_2 \mathrm{P}_b} x_3$, with $x_2 \in \mathcal{X}_2$ and $x_3 \in \mathcal{X}_3$. P_b denotes the total transmit power at the BS for users. The a_1 and a_2 are power coefficients which are assigned according to channel gain conditions, therefore $a_2 > a_1$ and $a_1 + a_2 = 1$, and $\mathcal{X}_2$ and $\mathcal{X}_3$ are constellation points of users $\mathcal{U}_2$ and $\mathcal{U}_3$, respectively.

TABLE 3.1: Nomenclature

Definition	**Parameter**
Number of transmit antennas at BS	N_{t}
Number of receive antennas at each user	N_{r}
Number of passive reflecting elements	N
Modulation order	M
User-1	$\mathcal{U}_1$
Near user (NU)	$\mathcal{U}_2$
Far user (FU)	$\mathcal{U}_3$
The channel between the BS to RIS	$\mathbf{H}$
The channel between the RIS to users	$\mathbf{G}_k$
Superposed signal at BS	$\mathbf{x}$
The constellation points	$\mathcal{X}_K$
The power coefficients are assigned for NOMA users	a_k
Additive white Gaussian noise for k receiver	$\mathbf{n}_k$
The channel coefficients between the l-th reflecting elements and t-th transmit antenna	$h_{l,t}$
The channel coefficients between the l-th reflecting elements and i-th k th user receive antenna	$g^k_{l,i}$
Phase matrix	$\mathbf{\Phi}$
The reflection coefficient of a lth element of RIS panel	β_l
The phase is adjusted according to CIRs between BS to RIS and RIS to user	ϕ_l
Phase between the l-th reflecting elements and t-th transmit antenna	$\varphi_{l,t}$
Phase between the l-th reflecting elements and i-th k th user receive antenna	$\psi^k_{l,t}$
The received signal at kth user	$\mathbf{y}_k$
Decoding antenna index at user-1	$\hat{t}$
Applying SIC at NU user	$\mathbf{y}_{2,\mathrm{SIC}}$
Decoding symbols for k user by using ML detector	$\hat{\mathrm{x}}_k$

3.2.1 Detection of User-1 ($\mathcal{U}_1$) Signal

The information of $\mathcal{U}_1$ is mapped to only TA index, and it's received signal $\mathbf{y}_1$ is expressed as

$$\mathbf{y}_1 = \mathbf{G}_1\mathbf{\Phi}\mathbf{H}\mathbf{x} + \mathbf{n}_1 \in \mathbb{C}^{N_\mathrm{r}\times 1}, \tag{3.3}$$

where, $\mathbf{n}_1 \sim \mathcal{CN}(0, N_0\mathbf{I}_{\mathbf{N}_\mathrm{r}})$ is additive white Gaussian noise (AWGN) vector with zero mean and variance N_0, the elements of channel matrices, $\mathbf{H}$ and $\mathbf{G}_k$ are given by $|h_{l,t}|e^{-j\varphi_{l,t}}$ and $|g^k_{l,i}|e^{-j\psi_{l,i}}$, respectively, where $\{l = 1, 2, ...N\}$, $\{t = 1, 2, ...N_\mathrm{t}\}$, $\{i = 1, 2, ...N_\mathrm{r}\}$, and $k = 1, 2, 3$. $h_{l,t}$ represents the channel coefficients between the l^{th} reflecting elements and t^{th} transmit antenna with phase $\varphi_{l,t}$ and $g^k_{l,i}$ is channel coefficients between the l^{th} reflecting elements and i^{th} receive antenna with phase $\psi^k_{l,i}$ for k^{th} user. The $\mathbf{\Phi}$ is a diagonal matrix, which is represents as $\mathbf{\Phi} = \mathrm{diag}[\beta_1 e^{j\phi_1}, \beta_2 e^{j\phi_2}, \ldots, \beta_N e^{j\phi_N}]$, where $\phi_l = \varphi_{l,t} + \sum_{k=1}^{K} \psi^k_{l,i}$ to maximize overall system performance and β_l denotes the reflection coefficient. In general $\beta_l \in (0, 1)$ depends on the surface material. However, we consider $\beta_l = 1$ for all the elements [76, 77].

The equation (3.3) is rewritten as,

$$\mathbf{y}_1 = \mathbf{G}_1\mathbf{\Phi}\mathbf{h}_t + \mathbf{n}_1 \in \mathbb{C}^{N_\mathrm{r}\times 1}, \tag{3.4}$$

where, $\mathbf{h}_t = \mathbf{H}\mathbf{x} \in \mathbb{C}^{N\times 1}$, which is an activated TA vector. Therefore TA index is estimated using maximum likelihood function (ML) which is given as [78],

$$\hat{t} = \arg \min_{t\in\{1,\ldots,N_\mathrm{t}\}} \|\mathbf{y}_1 - \mathbf{G}_1\mathbf{\Phi}\mathbf{h}_t\|_2^2 \tag{3.5}$$

where, $\hat{t}$ is an estimate of t. The user $\mathcal{U}_1$ recovers information bits $\log_2(N_t)$ from $\hat{t}$. For example, $\hat{t} = 1$ denotes 00 data symbols for $N_t = 4$.

3.2.2 Detection of NOMA Users $\mathcal{U}_2$ and $\mathcal{U}_3$ Signal

The NOMA users are carrying information through an activated TA with constellation symbols. The $\mathcal{U}_2$ is NU, and its signal decodes using SIC-based detection. The received signal at NU is expressed as,

$$\mathbf{y}_2 = \mathbf{G}_2\mathbf{\Phi}\mathbf{H}\mathbf{x} + \mathbf{n}_2 \in \mathbb{C}^{N_\mathrm{r}\times 1} \tag{3.6}$$

where $\mathbf{n}_2 \sim \mathcal{CN}(0, N_0\mathbf{I}_{\mathbf{N}_\mathrm{r}})$ is AWGN vector. We consider $|\mathbf{G}_2\mathbf{\Phi}\mathbf{H}| \gg |\mathbf{G}_3\mathbf{\Phi}\mathbf{H}|$.

The ML detection of the FU $\mathcal{U}_3$ at $\mathcal{U}_2$ is expressed as,

$$\hat{\mathrm{x}}_3^{\mathrm{NU}} = \arg \min_{\mathrm{x}_3\in\mathcal{X}_3, t\in\{1,\ldots,N_\mathrm{t}\}} \|\mathbf{y}_2 - \mathbf{G}_2\mathbf{\Phi}\mathbf{H}\mathbf{x}\|_2^2. \tag{3.7}$$

After perfect SIC, the received signal $\mathbf{y}_2$ is expressed as,

$$\mathbf{y}_{2,\mathrm{SIC}} = \mathbf{y}_2 - \mathbf{G}_2\mathbf{\Phi}\mathbf{H}\eta, \tag{3.8}$$

where, $\eta = [\underbrace{0,\ldots,0}_{(t-1)}, \sqrt{a_2 P_b}\hat{\mathrm{x}}_3^{\mathrm{NU}}, \underbrace{0,\ldots 0}_{(N_\mathrm{t}-t)}]$ is the FU's decoded vector at the $\mathcal{U}_2$. The NU's symbol is decoded from the $\mathbf{y}_{2,\mathrm{SIC}}$ as,

$$\hat{\mathrm{x}}_2^{\mathrm{NU}} = \arg \min_{\mathrm{x}_2\in\mathcal{X}_2, t\in\{1,\ldots,N_\mathrm{t}\}} \|\mathbf{y}_{2,\mathrm{SIC}} - \mathbf{G}_2\mathbf{\Phi}\mathbf{H}\mathbf{x}\|_2^2. \tag{3.9}$$

Next, the received signal $\mathbf{y}_3$ at FU is expressed as,

$$\mathbf{y}_3 = \mathbf{G}_3\mathbf{\Phi}\mathbf{H}\mathbf{x} + \mathbf{n}_3 \in \mathbb{C}^{N_\mathrm{r}\times 1} \tag{3.10}$$

where, $\mathbf{n}_3$ is AWGN vector. The ML detection for FU $\mathcal{U}_3$ is expressed as

$$\hat{\mathrm{x}}_3^{\mathrm{FU}} = \arg \min_{\mathrm{x}_3 \in \mathcal{X}_3, t \in \{1,\ldots,N_{\mathrm{t}}\}} \|\mathbf{y}_3 - \mathbf{G}_3 \mathbf{\Phi} \mathbf{H} \mathbf{x}\|_2^2. \tag{3.11}$$

Further, the NU signal is detected by considering an imperfect SIC which is expressed as,

$$\mathbf{y}_{2,\mathrm{ISIC}} = \mathbf{y}_2 - \mathbf{G}_2 \mathbf{\Phi} \mathbf{H} \kappa, \tag{3.12}$$

where, $\kappa = [\underbrace{0, \ldots, 0}_{(t-1)}, \sqrt{a_2 P_b}\hat{\mathrm{x}}_3^{\mathrm{FU}} + \varsigma, \underbrace{0, \ldots 0}_{(N_{\mathrm{t}}-t)}]$ is the FU's decoded information at the $\mathcal{U}_2$. ς denotes error in FU decoding which is assumed Gaussian distribution $\varsigma \sim \mathcal{CN}(0, N_\varsigma)$ [79]. Therefore, the NU signal $\mathbf{y}_{2,\mathrm{ISIC}}$ is expressed as,

$$\mathbf{y}_{2,\mathrm{ISIC}} = \mathbf{G}_2 \mathbf{\Phi} \mathbf{H} \varpi + \varsigma + \mathbf{n}_2 \in \mathbb{C}^{N_{\mathrm{r}} \times 1}. \tag{3.13}$$

where, $\varpi = [\underbrace{0, \ldots, 0}_{(t-1)}, \sqrt{a_1 P_b}\mathrm{x}_2^{\mathrm{NU}} +, \underbrace{0, \ldots 0}_{(N_{\mathrm{t}}-t)}]$. The NU's symbols are decoded from the $\mathbf{y}_{2,\mathrm{ISIC}}$ as,

$$\hat{\mathrm{x}}_2^{\varsigma} = \arg \min_{\mathrm{x}_2 \in \mathcal{X}_2, t \in \{1,\ldots,N_{\mathrm{t}}\}} \|\mathbf{y}_{2,\mathrm{ISIC}} - \mathbf{G}_2 \mathbf{\Phi} \mathbf{H} \mathbf{x}\|_2^2, \tag{3.14}$$

where $\hat{\mathrm{x}}_2^{\varsigma}$ denotes NU symbols using an imperfect SIC. We have also summarized users' detection in **Algorithm-1**

3.3 BEP Performance Analysis

In this section, the theoretical bit error probability (BEP) of the proposed downlink R-INOMA system using pairwise error probability (PEP) over flat Rayleigh fading channel is presented.

Algorithm 1 Users Detection in R-INOMA

Input: N_t, N_r, N and M.

for $iteration1 = 1, 2, \ldots,$ **SNR do**
  for $iteration2 = 1, 2, \ldots, bits$ **do**
    Assign antenna index N_t to $\mathbf{U}_1$
    Assign power coefficient to $\mathbf{U}_2$ and $\mathbf{U}_3$ $P_1 = 0.3$ and$P_2 = 0.7$
    Generate channels and phase are $\mathbf{H}$, $\mathbf{G}$ and $\mathbf{\Phi}$.
    Construct: $\mathbf{\Phi} = \text{diag}[\beta_1 e^{j\phi_1}, \beta_2 e^{j\phi_2}, \ldots, \beta_N e^{j\phi_N}]$.
    set $\beta_l = 1 \forall l$ and $\phi_{l(\max)} = \varphi_{l,t} + \psi^1_{l,i} + \psi^2_{l,i} + \psi^3_{l,i}$.
    ML Decoding for $\mathbf{U}_1$,
    for $t \leftarrow 1$ to N_t **do**
      $\hat{t} = \left\|\mathbf{y}_1 - \mathbf{G}_1^H \mathbf{\Phi} \mathbf{h}_t\right\|^2$
    end for
    Applied Perfect SIC at $\mathbf{U}_2$, after that applied ML decoder
    $\hat{\mathrm{x}}_2 = \left\|\mathbf{y}_{2,\text{SIC}} - \mathbf{G}_2^H \mathbf{\Phi} \mathbf{H} \eta\right\|^2$.
    ML Decoding for $\mathbf{U}_3$
    $\hat{\mathrm{x}}_3 = \left\|\mathbf{y}_3 - \mathbf{G}_3^H \mathbf{\Phi} \mathbf{H} \mathbf{x}\right\|^2$.
  end for
  Calculate BER for $\mathbf{U}_1$, $\mathbf{U}_2$ and $\mathbf{U}_3$.
  BER of $\mathbf{U}_1$ is sum (**xor**(bits,decoded))/total bits
  Similarly for $\mathbf{U}_2$ and $\mathbf{U}_3$.
end for

3.3.1 Performance Analysis of *User-1* ($\mathcal{U}_1$)

The PEP between the TA index t and erroneously detected index $\hat{t}$, under the condition on $\mathbf{G}_1$, $\mathbf{\Phi}$, and $\mathbf{h}_t$ is represented as,

$$\begin{aligned} &\Pr\left(t \to \hat{t} \,|\mathbf{G}_1, \mathbf{\Phi}, \mathbf{h}_t\right) = \Pr\left(\left|\mathbf{y}_1 - \mathbf{G}_1 \mathbf{\Phi} \mathbf{h}_t\right|^2 > \left|\mathbf{y}_1 - \mathbf{G}_1 \mathbf{\Phi} \mathbf{h}_{\hat{t}}\right|^2\right) \\ &= \Pr\Bigg(\underbrace{-\left|\mathbf{G}_1 \mathbf{\Phi}\left(\mathbf{h}_t - \mathbf{h}_{\hat{t}}\right)\right|^2 - 2\Re\left\{\mathbf{n}_1^* \left[\mathbf{G}_1 \mathbf{\Phi}(\mathbf{h}_t - \mathbf{h}_{\hat{t}})\right]\right\}}_{\mathcal{D}} > 0\Bigg) = \Pr\left(\mathcal{D} > 0\right), \end{aligned} \tag{3.15}$$

where, $\mathcal{D}$ is a Gaussian random variable with mean and variance as

$$\mathbb{E}\{\mathcal{D}\} = -\left|\mathbf{G}_1 \mathbf{\Phi}\left(\mathbf{h}_t - \mathbf{h}_{\hat{t}}\right)\right|^2, \text{Var}\{D\} = 2N_0 \left|\mathbf{G}_1 \mathbf{\Phi}\left(\mathbf{h}_t - \mathbf{h}_{\hat{t}}\right)\right|^2. \tag{3.16}$$

Then, the conditional PEP represents in terms of Q-function as

$$\Pr\left(t \to \hat{t} \,|\mathbf{G}_1, \mathbf{\Phi}, \mathbf{h}_t\right) = Q\left(\sqrt{\frac{\left|\mathbf{G}_1 \mathbf{\Phi}\left(\mathbf{h}_t - \mathbf{h}_{\hat{t}}\right)\right|^2}{2N_0}}\right). \tag{3.17}$$

Further, we denote $Z = \mathbf{G}_1 \mathbf{\Phi}\left(\mathbf{h}_t - \mathbf{h}_{\hat{t}}\right)$ and it can be expanded as

$$Z = \left(\sum_{l=1}^{N} g_{l,i}^1 (h_{l,t} - h_{l,\hat{t}}) e^{j[\phi_l - (\psi_{l,i}^1 + \varphi_{lt} - \varphi_{l\hat{t}})]}\right). \tag{3.18}$$

The channels coefficients of $\mathcal{U}_1$ are $h_{l,t}$ and $g_{l,i}^1$ are iid Rayleigh distributed with mean and variance of $\mathrm{E}[h_{l,t} g_{l,i}^1] = \frac{\pi}{4}$, and $\mathrm{VAR}[h_{l,t} g_{l,i}^1] = (1 - \frac{\pi^2}{16})$, respectively. By applying the central limit theorem (CLT) for large number reflecting elements $N \gg 1$, Z is approximated Gaussian distributed with the parameters $\mathbb{E}[Z]$[1] $= \frac{N\pi}{4}$, $\mathrm{Var}[Z] = N(1 - \frac{\pi^2}{16})$. The average PEP (APEP) is expressed as,

$$\overline{P}_e^1 = \int_0^\infty Q\left(\sqrt{\frac{\xi}{2N_0}}\right) f_\xi(\xi) d\xi, \tag{3.19}$$

where $\xi = |Z|^2$. By applying non noncentral chi-square distribution, APEP represents as

$$\overline{P}_e^1 = \frac{1}{\pi} \int_0^{\pi/2} M_\xi\left(-\frac{1}{4N_0 \sin^2 \lambda}\right) d\lambda, \tag{3.20}$$

where $M_\xi(\cdot)$ denotes moment generating function (MGF) associate with random variable ξ and is represented as [81]

$$M_\xi(\upsilon) = \left(\frac{1}{1 - \frac{\upsilon N(16-\pi^2)}{32N_0}}\right)^{\frac{1}{2}} \exp\left(\frac{\frac{\upsilon N^2 \pi^2}{32N_0}}{1 - \frac{\upsilon N(16-\pi^2)}{32N_0}}\right). \tag{3.21}$$

[1]Imperfect phase cancellation case mean can be different [80].

By substituting the equation (3.21) in the equation.(3.20), and the error probability $\overline{P}_e^1$ is obtained as

$$\overline{P}_e^1 = \frac{1}{\pi}\int_0^{\pi/2}\left(\frac{1}{1+\frac{N(16-\pi^2)}{32N_0\sin^2\lambda}}\right)^{\frac{1}{2}}\exp\left(\frac{-\frac{N^2\pi^2}{32N_0\sin^2\lambda}}{1+\frac{N(16-\pi^2)}{32N_0\sin^2\lambda}}\right)d\lambda. \tag{3.22}$$

Further, by considering $\lambda = \pi/2$ the upper bound of $\overline{P}_e^1$ is expressed as

$$\overline{P}_e^1 \leq \frac{1}{2}\left(\frac{1}{1+\frac{N(16-\pi^2)}{32N_0}}\right)^{\frac{1}{2}}\exp\left(\frac{-\frac{N^2\pi^2}{32N_0}}{1+\frac{N(16-\pi^2)}{32N_0}}\right). \tag{3.23}$$

Therefore, the ABEP $\overline{P}_b$ is represented as $\overline{P}_b \leq \frac{N_t}{2}\overline{P}_e^1$.

Asymptotic Diversity: The received signal is expressed as $S = \sum_{l=1}^{N}|g_{l,i}^1||h_{l,t}|$ [82] and instantaneous SNR, $\gamma = E_s\frac{S^2}{N_0} = \gamma_0 S^2$, where, $\gamma_0 = E_s/N_0$. At high SNR probability density function (pdf) of S is written as $f_S(s) \approx \frac{4^N s^{2N-1}}{\Gamma(2N)}$, [82] where $\Gamma(\cdot)$ denotes the Gamma function and the pdf of γ is written as, $f_\gamma(\gamma) \approx \frac{4^N\gamma^{N-1}}{2\Gamma(2N)\gamma_0^N}$. Therefore, the upper bound of APEP is expressed as

$$\overline{P}_e^1 \leq \frac{2^{N+2}\Gamma(N)}{2\pi\Gamma(2N)a^n\gamma_0^N} \tag{3.24}$$

Hence, $\overline{P}_e^1 \propto \gamma_0^{-N}$, and the maximum diversity order is N.

3.3.2 Performance Analysis of NOMA Users

In this section, the ABER performance of NOMA users, $\mathcal{U}_2$ and $\mathcal{U}_3$ analyzed. The $\mathcal{U}_3$ is far from RIS, and its channel coefficients are represented as, $h_{l,t}$ and $g_{l,i}^3$. The product $h_{l,t}g_{l,i}^3$ is Rayleigh distributed with mean and variance $\mathbb{E}[h_{l,t}g_{l,i}^3] = \frac{\pi}{8}$, $\mathrm{Var}[h_{l,t}g_{l,i}^3] = (\frac{16-\pi^2}{32})$ respectively. The $\mathcal{U}_3$ receives SC symbols from RIS, and using BPSK modulation and all symbols are equally likely probable. $\mathcal{U}_3$ information

is extracted by using ML detection and a symbol is detected erroneous if ($n_I \geq \sqrt{\epsilon_1}\mathcal{H}_3 - \sqrt{\epsilon_2}\mathcal{H}_3$), where n_I is in-phase component of AWGN, which is higher than the in-phase component of symbol amplitude [83]. The quadrature component n_Q does not effect $\mathcal{U}_3$ decision, since $\mathcal{U}_3$'s decision symbol depends on real component of the received signal. Further, $\epsilon_1 = a_1 \mathrm{P}_b$ and $\epsilon_2 = a_2 \mathrm{P}_b$ are power assigned for users $\mathcal{U}_2$ and $\mathcal{U}_3$ users, respectively. The $\mathcal{H}_3$ is channel between BS to $\mathcal{U}_3$ through RIS and is expressed as $\mathcal{H}_3 = \left(\sum_{l=1}^{N} g_{l,i}^3 h_{l,t}\right)^2$. Further, the error probability of the FU with ML detection is expressed as,

$$\mathrm{P}_e = \frac{1}{2}\left[\mathrm{Q}(\sqrt{\rho_1}) + \mathrm{Q}(\sqrt{\rho_2})\right] \tag{3.25}$$

where, ρ_1 and ρ_2 are the maximized SNR towards the $\mathcal{U}_3$ with different constellation points. The maximized SNRs of the user $\mathcal{U}_3$ are expressed as,

$$\rho_1 = \frac{|\mathcal{H}_3|^2(\sqrt{\epsilon_1} - \sqrt{\epsilon_2})^2}{N_0} \text{and } \rho_2 = \frac{|\mathcal{H}_3|^2(\sqrt{\epsilon_1} + \sqrt{\epsilon_2})^2}{N_0} \tag{3.26}$$

ABER $\overline{P}_e^3$ of the FU with BPSK modulation is expressed as [83],

$$\overline{P}_e^3 = \frac{1}{2}\left[\int_0^\infty Q\left(\sqrt{\rho_1}\right) f_{\rho_1}(\rho_1) d\rho_1 + \int_0^\infty Q\left(\sqrt{\rho_2}\right) f_{\rho_2}(\rho_2) d\rho_2\right], \tag{3.27}$$

By applying central limit theorem (CLT) for large number reflecting elements $N \gg 1$, the mean and variance of the channel, $\mathcal{H}_3$ are $\mathbb{E}[\mathcal{H}_3] = \frac{N\pi}{8}$, and $\mathrm{Var}[\mathcal{H}_3] = N(\frac{16-\pi^2}{32})$ respectively. Using MGF approach, the ABER is expressed as [81]

$$\overline{P}_e^3 = \frac{1}{2\pi}\left[\int_0^{\pi/2} M_{\rho_1}\left(-\frac{1}{2\sin^2\lambda}\right) d\lambda + \int_0^{\pi/2} M_{\rho_2}\left(-\frac{1}{2\sin^2\lambda}\right) d\lambda\right] \tag{3.28}$$

The MGFs for SNR with one degree of freedom are presented as,

$$M_{\rho_1}(\upsilon) = \left(\frac{1}{1-\frac{\upsilon N(16-\pi^2)(\sqrt{\epsilon_1}-\sqrt{\epsilon_2})}{16N_0}}\right)^{\frac{1}{2}} \exp\left(\frac{\frac{\upsilon N^2\pi^2(\sqrt{\epsilon_1}-\sqrt{\epsilon_2})}{32N_0}}{1-\frac{\upsilon N(16-\pi^2)(\sqrt{\epsilon_1}-\sqrt{\epsilon_2})}{16N_0}}\right) \text{ and} \tag{3.29}$$

$$M_{\rho_2}(\upsilon) = \left(\frac{1}{1-\frac{\upsilon N(16-\pi^2)(\sqrt{\epsilon_1}+\sqrt{\epsilon_2})}{16N_0}}\right)^{\frac{1}{2}} \exp\left(\frac{\frac{\upsilon N^2\pi^2(\sqrt{\epsilon_1}+\sqrt{\epsilon_2})}{32N_0}}{1-\frac{\upsilon N(16-\pi^2)(\sqrt{\epsilon_1}+\sqrt{\epsilon_2})}{16N_0}}\right). \tag{3.30}$$

After substituting (3.29) and (3.30) in (3.28), the ABER, $\overline{P}_e^3$ is expressed in (3.31) by considering the an upper bound at $\lambda = \pi/2$.

$$\begin{aligned}\overline{P}_e^3 \leq{}& \tfrac{1}{4}\left(\frac{1}{1+\frac{N(16-\pi^2)(\sqrt{\epsilon_1}-\sqrt{\epsilon_2})^2}{32N_0}}\right)^{\frac{1}{2}} \exp\left(\frac{\frac{-N^2\pi^2(\sqrt{\epsilon_1}-\sqrt{\epsilon_2})^2}{32N_0}}{1+\frac{N(16-\pi^2)(\sqrt{\epsilon_1}-\sqrt{\epsilon_2})^2}{32N_0}}\right) \\ &+\tfrac{1}{4}\left(\frac{1}{1+\frac{N(16-\pi^2)(\sqrt{\epsilon_1}+\sqrt{\epsilon_2})^2}{32N_0}}\right)^{\frac{1}{2}} \exp\left(\frac{\frac{-N^2\pi^2(\sqrt{\epsilon_1}+\sqrt{\epsilon_2})^2}{32N_0}}{1+\frac{N(16-\pi^2)(\sqrt{\epsilon_1}+\sqrt{\epsilon_2})^2}{32N_0}}\right)\end{aligned} \tag{3.31}$$

the user, $\mathcal{U}_2$ is near to the RIS, and its information is extracted by using perfect SIC. The channels coefficients $\mathcal{U}_2$ are represented as $h_{l,t}$ and $g_{l,i}^2$ and effective channel mean and variance as are $\mathbb{E}[h_{l,t}g_{l,i}^2] = \frac{\pi}{4}$, and $\text{Var}[h_{l,t}g_{l,i}^2] = (1-\frac{\pi^2}{16})$ respectively. The $\mathcal{U}_2$ receives superimposed symbols from the RIS. If the symbols of FU are decoded without error, the error probability is represents as,

$$P_e = \frac{1}{2}\left[2\text{Q}(\sqrt{\rho_3}) - \text{Q}(\sqrt{\rho_4})\right] \tag{3.32}$$

where ρ_3 and ρ_4 are the maximized SNR towards $\mathcal{U}_2$ with different constellation points, which are expressed as,

$$\rho_3 = \frac{|\mathcal{H}_2|^2(\sqrt{\epsilon_1})^2}{N_0} \text{ and } \rho_4 = \frac{|\mathcal{H}_2|^2(\sqrt{\epsilon_1}+\sqrt{\epsilon_2})^2}{N_0} \tag{3.33}$$

where $\mathcal{H}_2 = \left(\sum_{l=1}^{N} g_{l,i}^2 h_{l,t}\right)^2$. The ABER $\overline{P}_e^2$ of the NU, $\mathcal{U}_2$ is given as,

$$\overline{P}_e^2 = \left[\int_0^\infty Q\left(\sqrt{\rho_3}\right) f_{\rho_3}(\rho_3) d\rho_3 - \frac{1}{2}\int_0^\infty Q\left(\sqrt{\rho_4}\right) f_{\rho_4}(\rho_4) d\rho_4\right]. \tag{3.34}$$

The upper bound of ABER for user $\mathcal{U}_2$ is expressed in (3.35) by considering similar procedure as FU.

$$\begin{aligned}\overline{P}_e^2 \leq \frac{1}{2}\left(\frac{1}{1+\frac{N(16-\pi^2)(\sqrt{\epsilon_1})^2}{16N_0}}\right)^{\frac{1}{2}} \exp\left(\frac{\frac{-N^2\pi^2(\sqrt{\epsilon_1})^2}{32N_0}}{1+\frac{N(16-\pi^2)(\sqrt{\epsilon_1})^2}{16N_0}}\right) \\ -\frac{1}{4}\left(\frac{1}{1+\frac{N(16-\pi^2)(\sqrt{\epsilon_1}+\sqrt{\epsilon_2})^2}{16N_0}}\right)^{\frac{1}{2}} \exp\left(\frac{\frac{-N^2\pi^2(\sqrt{\epsilon_1}+\sqrt{\epsilon_2})^2}{32N_0}}{1+\frac{N(16-\pi^2)(\sqrt{\epsilon_1}+\sqrt{\epsilon_2})^2}{16N_0}}\right).\end{aligned} \tag{3.35}$$

Complexity: The complexity of the ML detector is defined as, $\mathcal{O}((N+M)N_t^2)$, where, M is the modulation order and N_t denotes the number of transmitting antennas. Moreover, the complexity of ML detector is increased as increasing of M, N, and N_t, because the ML detector extracts both modulation symbol and M and antenna index N_t simultaneously [53].

3.3.3 Sum-rate Analysis

In this subsection, the sum-rate of the proposed system is analyzed. The average sum-rate of the proposed R-INOMA system is expressed as,

$$\text{sum-rate} = \log_2(N_t)\left[1-\overline{P}_e^1\right] + \log_2(1+\text{SNR}_{\text{NU}}) + \log_2(1+\text{SINR}_{\text{FU}}) \text{ bits/sec/Hz}.$$

The sum-rate of R-INOMA system depends on the spatial domain user ($\mathcal{U}_1$) as well as NOMA users. The achievable rate of $\mathcal{U}_1$ is expressed as,

$$\mathcal{R}_1 = \log_2 \text{N}_t \text{ bits per frame}, \tag{3.36}$$

where, N_t is the number of transmit antennas and the sum-rate of $\mathcal{U}_1$ with the detection error is expressed as,

$$\mathcal{R}_1 = \log_2(N_t)\left[1 - \overline{P}_e^1\right], \tag{3.37}$$

where $\overline{P}_e^1$ is an average BEP. The $\mathrm{SNR}_{\mathrm{NU}}$ of NU is defined as,

$$\mathrm{SNR}_{\mathrm{NU}} = \frac{\mathrm{E}_1||\mathcal{H}_2||_2^2}{N_0} \text{ with } \mathrm{E}_1 = (\sqrt{\epsilon_1})^2(\sqrt{\epsilon_1}+\sqrt{\epsilon_2})^2, \text{ and} \tag{3.38}$$

The signal to interference plus noise ratio (SINR) FU is written as,

$$\mathrm{SINR}_{\mathrm{FU}} = \frac{||\mathcal{H}_3||_2^2\mathrm{E}_2}{||\mathcal{H}_3||_2^2\mathrm{E}_1 + N_0}, \text{ with } \mathrm{E}_2 = (\sqrt{\epsilon_1}-\sqrt{\epsilon_2})^2(\sqrt{\epsilon_1}+\sqrt{\epsilon_2})^2. \tag{3.39}$$

Therefore, the sum-rate depends on the reflecting elements, N. Further, the sum-rate in the conventional NOMA (C-NOMA) is expressed as,

$$\text{sum-rate}_{\mathrm{C-NOMA}} = \log_2\left(1 + \frac{a_1 P_b|h_1|^2}{N_0}\right) + \log_2\left(1 + \frac{a_2 P_b|h_2|^2}{a_1 P_b|h_2|^2 + N_0}\right) \text{bits/sec/Hz}, \tag{3.40}$$

where, h_1 and h_2 are the channel responses between the BS to NU and FU, respectively. Hence, the sum-rate of the proposed R-INOMA system is achieved better performnace the C-NOMA system.

3.3.4 Energy Efficiency

The energy efficiency (EE) of the R-INOMA is defined as [84],

$$\mathrm{EE} = \frac{\mathrm{B}.\mathcal{R}}{\mathcal{P}_T}, \tag{3.41}$$

where, B is bandwidth and $\mathcal{R}$ is an achievable rate. The $\mathcal{P}_T$ is the total power consumption of the system, which consists of both transmit power P_{s} and dissipation power P_{d} in hardware components. The required power for RIS dissipated system [85] is expressed as,

$$p_{\mathrm{R}} = \left(2^{\mathcal{R}} - 1\right) \frac{N_0}{(N\beta_l \mathcal{H}_2)^2}. \tag{3.42}$$

The total power consumption in the R-NOMA system is expressed as,

$$\mathcal{P}_T^{\mathrm{R}} = \frac{p_{\mathrm{R}}}{\nu} + P_{\mathrm{s}} + P_{\mathrm{d}} + NP_{\mathrm{e}}, \tag{3.43}$$

where, ν denotes the efficiency of the power amplifier and P_{e} is the power dissipation per element. The required power consumption for a conventional NOMA system is given as,

$$\mathcal{P}_T^{\mathrm{n}} = \frac{p_{\mathrm{n}}}{\nu} + P_{\mathrm{s}} + P_{\mathrm{d}}, \tag{3.44}$$

where, $p_{\mathrm{n}} = \left(2^{\mathcal{R}} - 1\right) \frac{N_0}{h}$, and h denotes the channel response between the BS tand user. Figure 3.2 shows the EE with respect to an achievable rate, $\mathcal{R}$ for the R-INOMA and a conventional NOMA system. The maximum EE is 6 bit/s/Hz for both the systems but after the increase in $\mathcal{R}$, EE decreases the NOMA system. The proposed R-INOMA has better EE at a higher achievable rate, as observed in Figure 3.2.

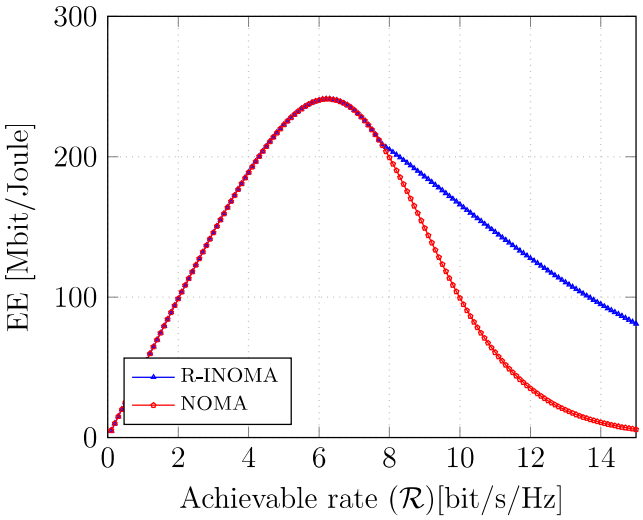

FIGURE 3.2: The energy efficiency as a function of the rate $\mathcal{R}$ with R-INOMA and NOMA system.

3.4 Simulation Results and Discussions

In this section, we present the simulations and analytical results for the proposed R-INOMA system. All users $\mathcal{U}_1$, $\mathcal{U}_2$, and $\mathcal{U}_3$ communicate over the flat Rayleigh fading channels [82] with $a_1 = 0.3$ and $a_2 = 0.7$, however, the power is splited between PD-NOMA users which is optimized by using the maximin fairness (MMF) criterion [86]. The data detection for all three users is carried out using ML detectors. However, user detection can be done by using a less-complex two-stage greedy detector [87]. Further, simulation parameters are summarized in Table 3.2.

The average BER performance of $\mathcal{U}_1$ is shown in Figure 3.3. The BER performance improved while increasing the number of the passive reflecting elements, N at the RIS due to enhancement in SNR of $\mathcal{U}_1$. The same performance is observed from the derived results at low SNR region because $P_e^1 \propto \exp\left(-\frac{N^2\pi}{16N_0}\right)$ and the error probability is inversely proportional to the reflecting element N.

TABLE 3.2: Simulation parameters

Parameter	Values
K	3
N_{t}	4
N_{r}	4
N	2 to 64
M	4 and 8
a_1	0.3
a_2	0.7
SNR_1	5dB
SNR_2	10dB
$\mathrm{SER}_{\mathrm{SNR}_1}$	0.0028
$\mathrm{SER}_{\mathrm{SNR}_2}$	0.0006
P_{s}= P_{d}	100 mW [84]
B	10 MHz
ν	0.5
β_l	1

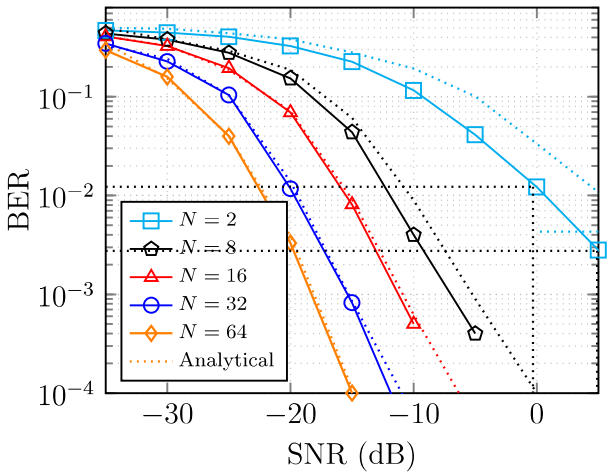

FIGURE 3.3: Average BER performance of R-INOMA with $N_{\mathrm{t}} = N_{\mathrm{r}} = 4$ for user-1 $\mathcal{U}_1$. Solid and dotted lines denote the simulation and analytical results, respectively.

The BER performance of NOMA-based users, $\mathcal{U}_2$ and $\mathcal{U}_3$ are shown in Figure 3.4 and Figure 3.5, respectively. Their BER performance is also improves by increasing N, and the BER of $\mathcal{U}_2$ is better than that of $\mathcal{U}_3$, because FU's interference is mitigated by using perfect SIC [88] at $\mathcal{U}_2$, as shown in Figure 3.4 and Figure 3.5. The analytical and the simulated results are closely matched for $\mathcal{U}_1$, $\mathcal{U}_2$, and $\mathcal{U}_3$ as shown

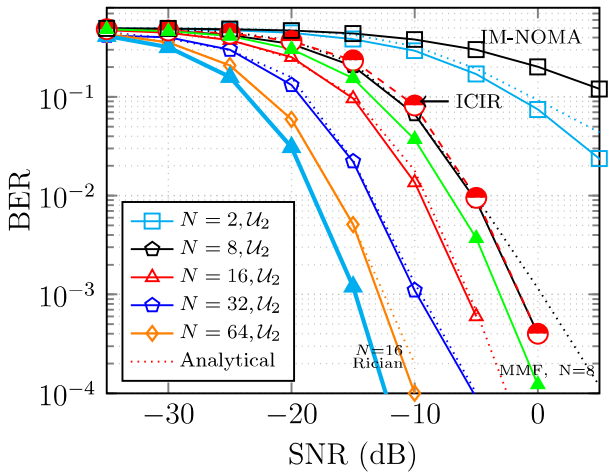

FIGURE 3.4: Average BER performance of R-INOMA with $N_\mathrm{t} = N_\mathrm{r} = 4$ for NU $\mathcal{U}_2$. Solid and dotted lines denote the simulation and analytical results, respectively.

Figures. 3.3, 3.4, 3.5, respectively, for higher values of N. However, a gap between the analytical and the simulated results exists for $N = 2, 8$ due to the limitation of CLT approximation. $\mathcal{U}_1$ has better BER performance over $\mathcal{U}_2$ and $\mathcal{U}_3$, as observed in results. the R-INOMA has better performance over INOMA ("IM-NOMA"), as observed in Figure 3.4 due to passive beamforming at RIS. The BER performance deteriorates in imperfect channel impulse response ("ICIR") case [89] as observed in Figure 3.4 for $N = 16$. Therefore, the quality of channel estimation determines the users' BER performance in the R-INOMA. Further, the BER performance improves in Rician fading (with Racian factor=1) between RIS and users as compared to Rayleigh fading, as observed in Figure 3.4 and Figure 3.5 due to the LOS path. Furthermore, MMF results show a better BER performance than fixed power allocation, as shown in Figure 3.4 due to adaptive power allocation between NOMA users.

The BER performance is improves for all three users while increasing the transmit antennas, N_t at BS for fixed number reflecting elements, $N = 32$ with BPSK modulation as shown in Figure 3.6. Figure 3.6 shows the BER performance of FU $\mathcal{U}_3$ for

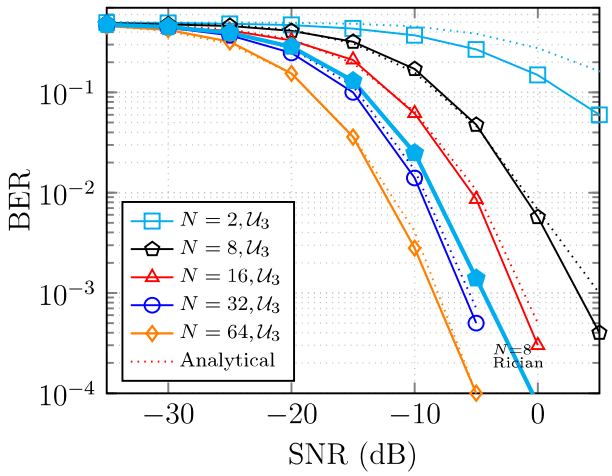

FIGURE 3.5: Average BER performance of R-INOMA with $N_{\mathrm{t}} = N_{\mathrm{r}} = 4$ for FU $\mathcal{U}_3$. Solid and dotted lines denote the simulation and analytical results, respectively.

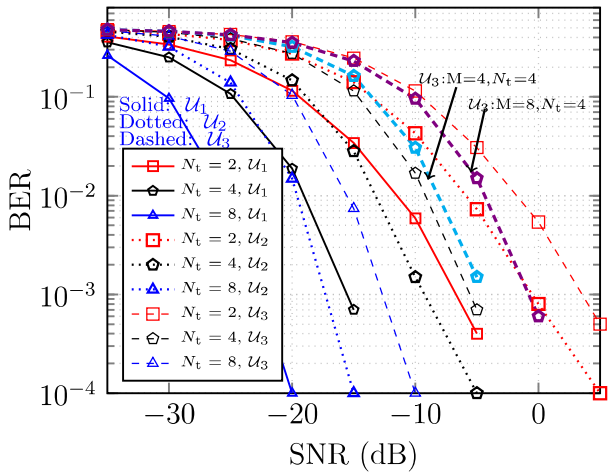

FIGURE 3.6: Average BER performance of R-INOMA with $N = 32$ and $M = 2$ for $N_{\mathrm{t}} = 2, 4, 8$ for all users $\mathcal{U}_1$, $\mathcal{U}_2$ and $\mathcal{U}_3$.

different modulation order M increases from 2 to 8 for a fixed reflecting elements $N = 32$ and $N_{\mathrm{t}} = 4$. Observe that the BER performance degrades by increasing modulation order M in Figure 3.6. Due to the probability of error for M-ary PSK is $P_e^3 \propto e^{(-\sin^2(\pi/M)N^2)}$. Therefore, the probability of detection error is increased with an increasing the modulation order, M.

Diversity order: The diversity order of the users, $\mathcal{U}_1$, $\mathcal{U}_2$ and $\mathcal{U}_3$ in R-INOMA is calculated by using the slope of the curves at high SNR region. The diversity order

equal to the negative slope of the curve which is defined as

$$\text{Slope} = \frac{10\left[\log_{10}\left(\frac{\text{BER}_{\text{SNR}_2}}{\text{BER}_{\text{SNR}_1}}\right)\right]}{\text{SNR}_2 - \text{SNR}_1}, \tag{3.45}$$

where, $\text{BER}_{\text{SNR}_1}$ and $\text{BER}_{\text{SNR}_2}$ denotes the BER at SNR_1 and SNR_2, respectively. Therefore, slope of the curve for $N = 2$ is:$\approx \frac{10\left[\log_{10}\left(\frac{0.0006}{.0028}\right)\right]}{10-5} = -1.338$ and for $N = 8$ is:$\approx -\frac{-10.1}{5} = -2.02$ shown in the Figure 3.3. Hence, the diversity order of R-INOMA at high SNR is between 1 and N, which validates the diversity of R-INOMA system. Since the diversity order of a user increases as N increases [80]. Further, slope of the curve for $N = 2$ is: $\approx -\frac{5.754}{10-5} = -1.151.$ and $\approx -\frac{-5.095}{5} = -1.019$ for $\mathcal{U}_2$ and $\mathcal{U}_3$, respectively in Figure 3.4 and Figure 3.5. Therefore, the diversity order of users is improves as N increases in R-INOMA.

Next, Figure 3.7 shows the NU's BER performance by applying an imperfect SIC. The imperfect SIC deteriorates the NU's performance as compared to the perfect SIC due to the presence of interference from the FU. Further, BER performance depends on the cancellation error ς in an imperfect SIC cases, as observed in Figure 3.7. Furthermore, the proposed R-INOMA system performance is better than the conventional INOMA system, due to improved received signal strength as shown in Figure 3.8. The R-INOMA significantly reduces BER at low SNR region, for example, BER=10^{-3} is achieved below 0 dB SNR for all three users as shown in Figure 3.8.

The average sum-rate performance [8, 47] of R-INOMA is shown in Figure 3.9 for $N = 2$ and 16. The phase angle of RIS are optimized: 1. to get the maximum sum-rate ("Opt."), 2. to maximize NU sum-rate ("NU Opt."), 3. to maximize FU sum-rate ("FU Opt."), and 4. by considering an average angle of FU and NU ("Average"), as shown in Figure 3.9. The proposed R-INOMA system has better

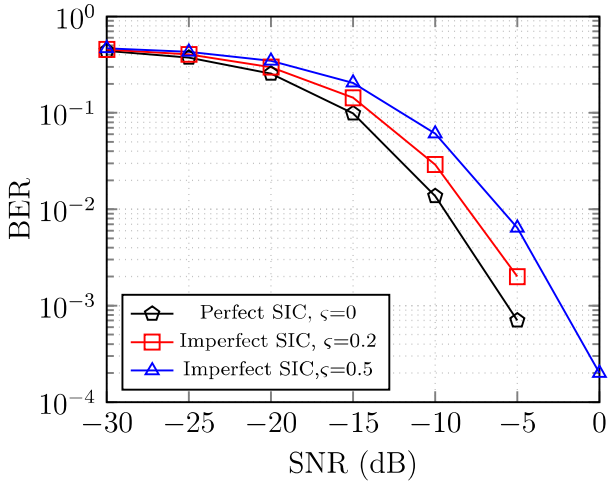

FIGURE 3.7: Average BER performance of R-INOMA using perfect and imperfect SIC at NU with BPSK modulation and fixed reflecting elements $N = 16$.

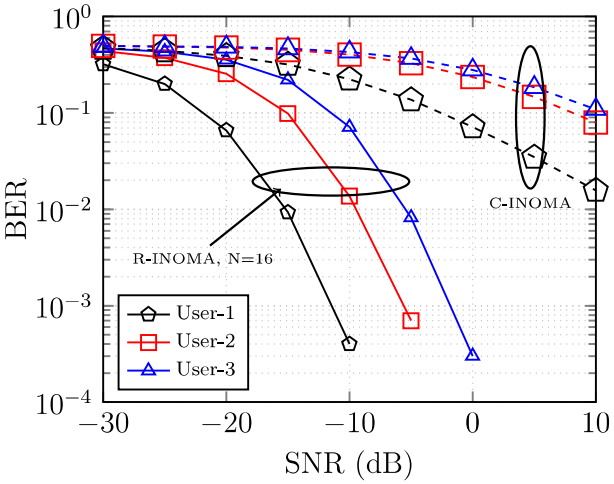

FIGURE 3.8: Average BER performance of proposed R-INOMA and C-INOMA.

sum-rate performance as compared to conventional INOMA [90], NOMA [91], and RIS-assisted OMA (R-IOMA) [86] systems, due to passive beamforming at the RIS panel, as observed in Figure 3.9. Further, the sum-rate depends on the number of reflected surfaces, N and angle optimization method in R-INOMA [80], as shown in Figure 3.9.

The results of the summary suggest that the performance of the proposed R-INOMA

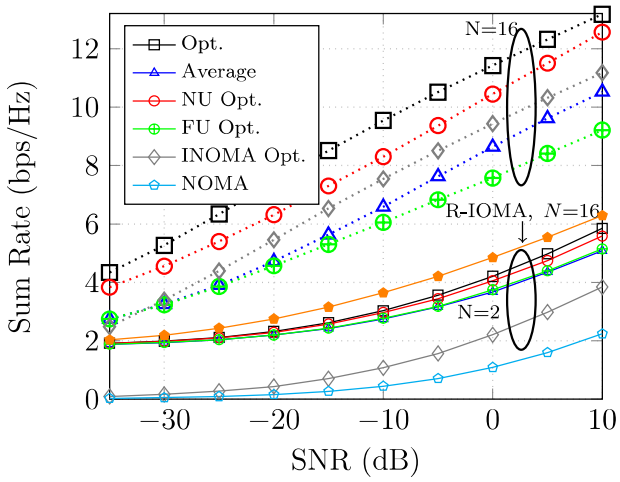

FIGURE 3.9: Sum-rate performance of the proposed R-INOMA with conventional NOMA and INOMA systems.

system is superior to that of C-NOMA, NOMA, and OMA. Additionally, the performance of the R-INOMA system is enhanced by increasing the number of reflecting elements and by supporting more users in each cluster.

3.5 Summary

In this chapter, a RIS-assisted INOMA (R-INOMA) system has been proposed to achieve a better BER performance at low SNR by reconfiguring the channel conditions of the users. Analytical expressions for the BER haven been derived for all three users and its performance have been validated through simulation and observed that they are closely matched. The proposed R-INOMA system has exhibited a high data rate transmission while increasing transmit antennas at BS with improved BER performance due to RIS. The BER performance has been improved with the number of reflecting elements at the RIS due to the coding gain and enhanced diversity order in R-INOMA. Further, the performance of the proposed R-INOMA shown that it can includes more users in a resource block, as compared to conventional RIS-NOMA

and also observed that the R-INOMA does not require any complex channel coding technique for a reliable communication system at the low SNR region due to passive beamforming at the RIS. Finally, in present study the deployment strategy of RISs, under the high scattering region not considered. Moreover, the aforementioned conditions are addressed by considering multiple RIS-assisted NOMA systems and to different deployment strategies in Chapter 4.